Phase-shift perfluorocarbon agents enhance high intensity focused ultrasound thermal delivery with reduced near-field heating

Linsey C. Phillips,[a] Connor Puett, Paul S. Sheeran, and Paul A. Dayton
Department of Biomedical Engineering, University of North Carolina at Chapel Hill, 109 Mason Farm Road, 304 Taylor Hall, CB 7575, Chapel Hill, North Carolina, 27599

G. Wilson Miller
Department of Radiology, University of Virginia, 480 Ray C. Hunt Drive, Charlottesville, Virginia, 22908

Terry O. Matsunaga
Department of Medical Imaging, University of Arizona, 1609 Ring Road, Tucson, Arizona, 85719

(Received 29 September 2012; revised 4 January 2013; accepted 8 January 2013)

Ultrasound contrast agents are known to enhance high intensity focused ultrasound (HIFU) ablation, but these perfluorocarbon microbubbles are limited to the vasculature, have a short half-life *in vivo*, and may result in unintended heating away from the target site. Herein, a nano-sized (100–300 nm), dual perfluorocarbon (decafluorobutane/dodecafluoropentane) droplet that is stable, is sufficiently small to extravasate, and is convertible to micron-sized bubbles upon acoustic activation was investigated. Microbubbles and nanodroplets were incorporated into tissue-mimicking acrylamide-albumin phantoms. Microbubbles or nanodroplets at 0.1×10^6 per cm^3 resulted in mean lesion volumes of 80.4 ± 33.1 mm^3 and 52.8 ± 14.2 mm^3 (mean $\pm$ s.e.), respectively, after 20 s of continuous 1 MHz HIFU at a peak negative pressure of 4 MPa, compared to a lesion volume of 1.0 ± 0.8 mm^3 in agent-free control phantoms. Magnetic resonance thermometry mapping during HIFU confirmed undesired surface heating in phantoms containing microbubbles, whereas heating occurred at the acoustic focus of phantoms containing the nanodroplets. Maximal change in temperature at the target site was enhanced by 16.9% and 37.0% by microbubbles and nanodroplets, respectively. This perfluorocarbon nanodroplet has the potential to reduce the time to ablate tumors by one-third during focused ultrasound surgery while also safely enhancing thermal deposition at the target site.
 [http://dx.doi.org/10.1121/1.4812866]

PACS number(s): 43.35.Ei, 43.35.Wa, 43.80.Sh [CCC] Pages: 1473–1482

I. INTRODUCTION

High intensity focused ultrasound (HIFU) is a non-invasive thermal ablation technique for the treatment of benign and malignant solid masses. In some countries, HIFU is approved to treat prostate cancer, and in the U.S., HIFU is approved by the Food and Drug Administration for the treatment of uterine fibroids (Ringold, 2004; Gedroyc and Anstee, 2007; Lukka *et al.*, 2011). HIFU is also under preclinical investigation as a potential treatment option for tumor malignancies located in brain, liver, prostate, pancreas, bone, and breast (Hill and terHaar, 1995; Kennedy, 2005; Pauly *et al.*, 2006; Wu *et al.*, 2007; Kinsey *et al.*, 2008; Maleke and Konofagou, 2008; Liberman *et al.*, 2009; Fischer *et al.*, 2010; Jang *et al.*, 2010; Maleke and Konofagou, 2010; McDannold *et al.*, 2010; Tempany *et al.*, 2011). Because HIFU requires no invasive procedures, radiation, or chemotherapy, it offers advantages over standard cancer therapy. Nevertheless, there are limitations to HIFU. A single ellipsoid volume (15–25 mm^3) is exposed to acoustic pulses with intensities above 10 000 W/cm^2. This power requirement carries a risk of uncontrolled tissue cavitation (Coussios *et al.*, 2007; Kyriakou *et al.*, 2011), and therefore exposure times are brief and separated by a period of heat dissipation. Hundreds of lesions and hours of therapy are often needed to treat a single tumor. Additionally, healthy tissue in the path of the high-energy acoustic beam is at risk for thermal injury (Mougenot *et al.*, 2011). Unintended heating can also occur near structures that attenuate or reflect ultrasound (air cavities or bone) (Connor and Hynynen, 2004; McDannold *et al.*, 2004). In response to these limitations, methods to lower the acoustic power requirements and treatment times to achieve ablation with HIFU are currently under investigation.

Research over the past decade has demonstrated that the presence of ultrasound contrast agents, or microbubbles, in a HIFU field substantially decreases the acoustic energy required to ablate tissue (Tran *et al.*, 2003; Liu *et al.*, 2006; Tung *et al.*, 2006; Yu *et al.*, 2006a; Yu *et al.*, 2006b; Stride and Coussios, 2010). Microbubbles are FDA-approved ultrasound contrast agents that are micron-sized gas (typically perfluorocarbon) bubbles with a polymer, protein, or lipid shell (Goldberg *et al.*, 1994). Insonated microbubbles resonate, generating additional heat, and collapse (cavitation), producing local shock waves that cause mechanical stress at

[a]Author to whom correspondence should be addressed. Electronic mail: linsey@email.unc.edu

the cellular level (Tran *et al.*, 2003; Xu *et al.*, 2005) thereby aiding tissue ablation. However, the clinical translation of microbubbles as an ablation mediator in treating tumors is fundamentally limited because microbubbles are (1) too large to extravasate from the vascular space (Ferrara *et al.*, 2007; Villanueva, 2008) and (2) have a very short half-life *in vivo* (minutes) (Mullin *et al.*, 2011). The production of stable microbubbles smaller than a micron is particularly challenging (Ganan-Calvo, 2004; Talu *et al.*, 2006; Xu *et al.*, 2006), and furthermore microbubbles much less than a micron respond poorly to low frequency ultrasound (Dayton *et al.*, 1999; Chomas *et al.*, 2001a; Chomas *et al.*, 2001b). Thus an alternative to traditional microbubbles is needed for focused ultrasound-mediated tumor applications.

An alternative to microbubbles is liquid perfluorocarbon (PFC)-based agents. Liquid PFC droplets can have a substantially longer circulation half-life than gas-filled microbubbles (Rapoport *et al.*, 2011). Furthermore, under sufficient acoustic energy, certain PFCs can be phase-shifted from liquid to gas form, resulting in microbubbles at the target site. Indeed, phase-change PFCs have been proposed as mediators for HIFU thermal delivery for this reason (Zhang and Porter, 2010; Zhang *et al.*, 2011).

Micron-sized liquid-based PFC agents have been studied extensively in ultrasound applications as agents for vascular occlusion (Kripfgans *et al.*, 2002; Kripfgans *et al.*, 2005). However, micron-sized PFC agents cannot access the extravascular space due to their size and thus would not accumulate in tumors. Hence the application of micron-sized PFC droplets in focused ultrasound surgery for tumor treatment is limited.

In response to the limitations inherent in the use of microbubbles and micron-sized droplets, efforts are now focused on nano-sized agents with the development of several techniques to synthesize stable liquid PFC nanodroplets (Kawabata *et al.*, 2010; Rapoport *et al.*, 2010; Zhang and Porter, 2010; Reznik *et al.*, 2011; Sheeran *et al.*, 2011a; Sheeran *et al.*, 2012; Singh *et al.*, 2012). When designed appropriately, PFC nanodroplets can be phase-shifted to gaseous microbubbles by the application of sufficient acoustic energy (Sheeran and Dayton, 2012). The acoustic parameters (HIFU intensity) required to initiate vaporization of the PFC droplet depend on the size of the droplet and its chemical composition (Rapoport *et al.*, 2009; Sheeran *et al.*, 2011b; Singh *et al.*, 2012). Taking advantage of temperature-pressure requirements for nanodroplet vaporization, our laboratory has synthesized unique phase-shift liquid nanodroplets using highly volatile PFCs, including decafluorobutane (DFB, C_4F_{10}, b.p. $= -2\,^{\circ}C$). Because these novel nanodroplets vaporize at a controlled pressure, they are expected to enhance thermal energy deposition only at the acoustic focus where the pressure is sufficiently high to vaporize nanodroplets into microbubbles.

We hypothesized that our new nanodroplet PFC formulation would thermally and spatially enhance HIFU ablation at the intended target site. Furthermore we predicted that these nanodroplets would provide more control over lesion size and placement than microbubbles and also enable shortening of heating times and/or lessening of delivered acoustic energy. We examined the thermal enhancement of the hybrid nanodroplets relative to standard microbubble formulations and agent free controls in a tissue mimicking acrylamide-albumin phantom in response to HIFU. Specifically, we assessed the relationship among agent concentration, acoustic pressure, and pulse length on vaporization threshold, lesion size, lesion location, and thermal enhancement. Finally, we examined temperature profiles during HIFU ablation by magnetic resonance (MR) thermometry.

II. MATERIALS AND METHODS

A. Microbubble preparation and condensation to nanodroplets

The phase-shift nanodroplets used in this study and their precursor microbubbles have PFC cores containing a mixture of DFB (C_4F_{10}) and dodecafluoropentane (DDFP, C_5F_{12}) encapsulated in a phospholipid shell. Lipids were purchased from Avanti Polar Lipids (Alabaster, AL), and PFCs were purchased from Fluoromed (Round Rock, TX). Lipid emulsions were formulated by dissolving 1,2-distearoyl-sn-glycero-3-phosphocholine and 1,2-distearoyl-sn-glycero-3-phosphoethanolamine-*N*-methoxy(polyethylene-glycol)-2000 in a 9:1 M ratio and a total lipid concentration of 1.0 mg/ml in a solution of phosphate-buffered saline (PBS), propylene glycol, and glycerol as previously described (Sheeran *et al.*, 2012). A total of 1.5 ml lipid mixture was added to a 3 ml glass vial, and the headspace of the vial was then gas-exchanged with a 1:1 mixture of DFB:DDFP gas. All microbubbles with a PFC core and a phospholipid shell arranged spontaneously during agitation using a Vialmix Shaker (Bristol-Myers-Squibb, NY, NY). Microbubble stock solutions contain approximately 10^{10} microbubbles/ml.

Nanodroplets were formed by the condensation of the precursor microbubbles as previously described (Sheeran *et al.*, 2011a). Briefly, the 3 ml vials containing microbubbles were immersed in a CO_2/isopropanol bath controlled to a temperature between $-5\,^{\circ}C$ and $-10\,^{\circ}C$ and swirled gently for approximately 1 min. The vials were connected to an adjustable air pressure source, and headspace pressure in the vial was increased until a change in the consistency was noted in the microbubble solution, indicating the onset of condensation. The combination of propylene glycol, glycerol, and PBS prevents freezing during the approximately 2 min exposure to sub-zero temperature. After condensation, the pressure source was removed from the vial, leaving a pressure head on the solution until further use. Assuming a direct conversion between the gas and liquid states, nanodroplet stock solutions also contain approximately 10^{10} nanodroplets/ml.

B. Nanodroplet and microbubble sizing

Microbubble concentration and size distributions were measured in triplicate using an Accusizer 780 (Particle Sizing Systems, Santa Barbara, CA) with a lower detection limit of 0.5 μm. Dynamic light scattering (Malvern Nano ZS, Malvern Instruments, Westborough, MA) with a measurement range of 0.3 nm to 6 μm diameters was used to assess

size distributions of the nanodroplets. The condensed nanodroplet solution was transferred to a cuvette immediately prior to sizing. Stability of the nanodroplets in stock solution was assessed by repeated sizing several hours/days after their condensation at 37 °C as performed previously (Sheeran *et al.*, 2012).

C. Tissue-mimicking phantoms

Acrylamide-albumin tissue mimicking phantom, similar to those previously described (Takegami *et al.*, 2004), were created from an 8:7:5 mixture of an aqueous acrylamide solution, liquid egg white, and deionized water, respectively. The advantage of these phantoms is their near transparency until heated above 60 °C. Upon reaching this ablation threshold, the egg whites are permanently denatured, creating a visibly opaque lesion. Controlled volumes (0.0025–1 μl/ml of phantom material) of the stock microbubble or nanodroplet solutions were added to the phantom acrylamide solution to generate various agent concentrations within the phantoms. Agents were gently dispersed throughout the degassed acrylamide solution prior to polymerization via the addition of 1% vol./vol. of 10% ammonium persulfate and 0.4% vol./vol. tetramethylethylenediamine, and then the solution was poured into an angled cylindrical mold. The top and bottom diameters of the phantoms were 3 and 4.1 cm, respectively, with a height of 1.5 cm, resulting in a total volume of 10 ml. Because the stock solutions of nanodroplets and microbubbles contained approximately 10^{10} agents/ml, the final concentrations of nanodroplets and microbubbles in the tissue-mimicking phantoms ranged from 10^4 to 10^7 agents/ml. For comparison, the prescribing information for Definity® suggests injecting 1.2×10^8 microbubbles/kg (or roughly 1.2×10^5 microbubbles/g), and we incorporate roughly the same number per gram of phantom tissue when 0.01 μl of stock agent solution is added per milliliter of phantom material. From this point on, the nanodroplet or microbubble concentration will be referenced by the microliters (μl) of stock solution added per milliliter of phantom material. All phantoms were used within 48 h of their generation.

D. Tumor-mimicking model for HIFU ablation

To simulate a tumor surrounded by healthy tissue, the 10 ml phantom (mimicking the tumor mass) was placed within an agent-free gellan gum mold and separated from the ultrasound transducer by a 10 mm thick degassed, agent-free acrylamide-albumin gel cap (Fig. 1). This mold and cap (mimicking healthy tissue surrounding the tumor) were positioned below the HIFU transducer such that the center of the phantom was at the focal point of the HIFU beam. The agent-free gels encasing the phantom allowed for assessment of thermal damage outside of the intended ablation area. The tissue mimicking gels and mold were placed in a bath of circulating degassed water to maintain a constant temperature of 37 °C. An acoustic absorbent pad was placed below the bottom mold to minimize possible sound wave reflection off the acrylic floor of the water bath.

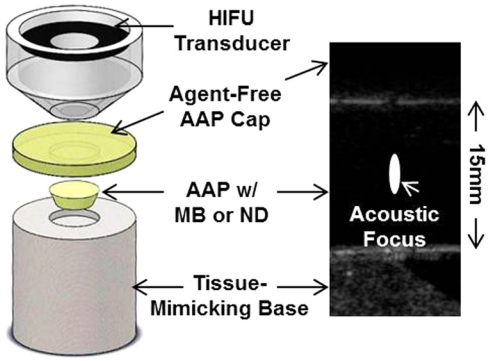

FIG. 1. (Color online) (Left) A tissue-mimicking albumin-acrylamide phantom (AAP) containing nanodroplets was positioned between a tissue-mimicking gellan gum base below and an agent free albumin-acrylamide cap above. High intensity focused ultrasound (HIFU) was directed toward the center of the phantom from above. The image on the right is a representative pre-HIFU acoustic image of the aligned phantoms with a nanodroplet phantom in the center. The white ellipse denotes the location and approximate dimensions of the acoustic focus where ablation was performed. Notice that no agents are visible within the phantom prior to HIFU.

E. Focused ultrasound

HIFU was delivered by a spherically focused, eight-element, 1.2 MHz, transducer array (Imasonic, Voray-sur-l'Ognon, France) driven by a therapy imaging probe system (TIPS) (Philips Research North America, Briarcliff Manor, NY). The diameter and focal length of the transducer were both 80 mm. Continuous-wave HIFU was applied at 1 MHz in all studies and delivered at peak negative pressures (PNPs) of 1, 2, 3, and 4 MPa. Calibration at each pressure was determined using a needle hydrophone (Onda HNA-0400, Sunnyvale, CA) in a degassed water bath. The applied acoustic intensities are approximately 30 W/cm^2 at 1 MPa, 125 W/cm^2 at 2 MPa, 280 W/cm^2 at 3 MPa, and 500 W/cm^2 at 4 MPa. Precise axial and lateral positioning of the focal point (TIPS focal zone: $1 \times 1 \times 6$ mm) was achieved by using a three-dimensional (3-D) motion stage.

F. Acoustic imaging of the onset of vaporization and the volume of the vaporization field

Liquid nanodroplets at the low concentrations used in this study are not acoustically detectable by conventional ultrasound imaging prior to vaporization. Therefore both control phantoms and those containing nanodroplets are acoustically transparent. To date, nanodroplet vaporization has most often been assessed in small capillary tubes containing aqueous solutions by the passive detection of emitted acoustic signatures. In this study, nanodroplet vaporization was assessed directly in the tissue-mimicking gel by acoustic imaging of the echogenic microbubble cloud (vaporization field) that forms during the application of HIFU. In order to determine the onset of vaporization, acoustic imaging was performed after the application of continuous-wave HIFU at pressures of 1, 2, 3, and 4 MPa to phantoms containing 0.1 μl of nanodroplet stock per ml for exposure times ranging from 2 ms to 20 s.

Each phantom was sonicated only once and then immediately imaged using a 15L8 transducer probe with a

Siemens Sequoia scanner (Siemens, Mountain View, CA) operating in B-mode at 14 MHz. Testing was performed in triplicate. Dicom images were analyzed offline by IMAGEJ software (http://rsbweb.nih.gov/ij/). An ellipse region of interest (ROI) measuring the size of the known focal beam dimensions was drawn within each image at the site of vaporization. A second equally sized ellipse was drawn on the unaffected region of the phantom, at least 5 mm to the left or right, but within the same image, as a measure of background intensity. Pixel intensity in each ellipse was measured and the mean calculated. The background mean was subtracted from the mean pixel intensity in the vaporization ROI, and the pixel intensity was plotted against time to determine the onset of vaporization.

In a separate set of experiments, the final volume of the vaporization field (microbubble cloud) was determined in phantoms containing 0.05, 0.1, 0.25, or 1.0 μl of nanodroplet stock per milliliter that were insonated by continuous-wave HIFU for 20 s at 1, 2, 3, and 4 MPa. The phantoms were imaged immediately after HIFU application using the 15L8 transducer probe and Siemens Sequoia scanner operating in B-mode at 14 MHz (Fig. 1). The width and height of the vaporization field were measured, and the corresponding vaporization field volume was estimated as an ellipsoid and calculated as described in the following section.

G. Lesion formation as a function of concentration of agents and of pressure

Acrylamide-albumin phantoms containing between 0.0025 and 1 μl of stock nanodroplet or microbubble solution per milliliter of phantom material were insonated by continuous wave HIFU for 20 s at 1 MHz using PNPs of 1, 2, 3, or 4 MPa. All experiments were repeated in at least triplicate. Ablation lesions were visible as opaque regions in the otherwise transparent phantom. Phantoms were cut by scalpel, and the maximum height (vertical axis) and width (lateral axis) of each ablation lesion was determined by direct visualization and measured by calipers. The volume of the ellipsoid lesion was calculated using the formula

$$\text{volume} = (4/3) * \pi * (\text{maximum height}/2) * (\text{maximum width}/2)^2. \quad (1)$$

H. MR thermometry

MR thermometry was applied to investigate thermal deposition in phantoms containing nanodroplets and microbubbles. MR imaging was performed at 3T (Magnetom Trio, Siemens Healthcare, Malvern, PA) using a custom 2-in. square, single-loop, receive-only RF coil (FUS Instruments, Toronto, Canada). Ultrasound sonication was performed inside the scanner using an MR-compatible system consisting of a focused 1 MHz transducer (75 mm diameter, F# = 0.8) with three-axis motor control (RKO-100, FUS Instruments). Albumin-acrylamide gel phantoms containing no agent (control), nanodroplets (0.005 μl/ml, 0.01 μl/ml, or 0.1 μl/ml), or microbubbles (0.005 μl/ml or 0.01 μl/ml) were insonated by continuous wave HIFU at 1.1 MHz with a PNP of 4.69 MPa (20 W) for 60 s. For each application of HIFU, the temperature was monitored either in a single vertical slice or in three parallel horizontal (perpendicular to the axis of the acoustic beam) slices (see Fig. 2). The center-to-center slice spacing was 4.5 mm for the horizontal scans.

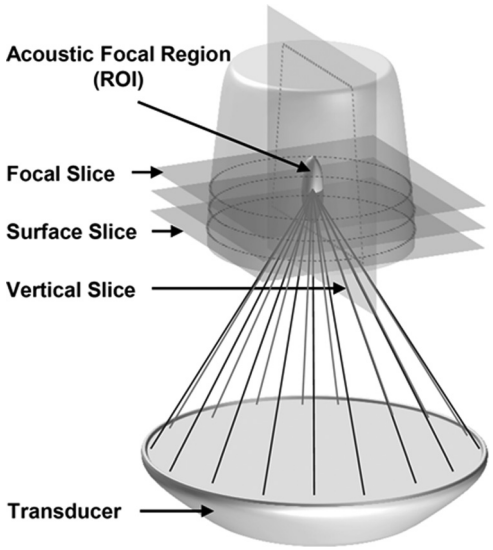

FIG. 2. Schematic representation of the AAP position above the HIFU transducer. The acoustic focus was positioned directly in the center of the phantom. Horizontal MR slices were collected at the focus, at the surface of the phantom, and in between these two slices. During separate scans, vertical slices were collected parallel to the axial length of the acoustic focus.

All MR images were acquired using a 2D multi-slice, spoiled gradient-echo pulse sequence with the following parameters: TR/TE = 39/5 ms, field of view = 51 × 102 mm, matrix = 64 × 128, in-plane resolution = 0.8 × 0.8 mm, readout bandwidth = 220 Hz/pixel, flip angle = 25°, slice thickness = 2.5 mm, scan time = 2.5 s per image set. For each ultrasound application, 50 consecutive image sets were acquired back to back for a total scan time of 2 min and 5 s. Ultrasound sonication was initiated 5 s into the MR scan (immediately following acquisition of the second image set), lasted for 60 s, and imaging continued for an additional 60 s during cool-down.

Maps of the temperature evolution during and post each ultrasound application were computed from the MR images using the proton resonance frequency shift method (Hindman, 1966; Ishihara *et al.*, 1995), similar to previously described thermometry studies (Germain *et al.*, 2001; Rieke and Pauly, 2008). Specifically, the temperature change during the scan was computed from the phase difference between the second image (acquired immediately before starting the sonication) and each subsequent image of the scan, assuming −0.01 ppm/°C temperature sensitivity at the actual scanner field strength of 2.89 T.

I. Statistical analysis

Data sets were evaluated using Student's *t*-tests in the case of paired means and were evaluated by one-way analysis of variance (ANOVA) when more than two groups were compared. All results are reported as the mean of that data

and its corresponding standard deviation. In cases where n was not equal across data sets, standard error is reported. All experiments were performed in at least triplicate, and p values of <0.05 were considered to be statistically significant.

III. RESULTS

A. Nanodroplet and microbubble size

The average diameter of the nanodroplet population was measured to be 240 ± 65 nm by dynamic light scattering. Nanodroplets remained stable in solution at 37 °C for at least 48 h after condensation. As assessed by laser light diffraction, the mean microbubble diameter was 0.98 ± 0.68 μm.

B. Onset of vaporization

In phantoms containing 0.1 μl of stock nanodroplets, vaporization of the nanodroplets at the HIFU focus generated a central bubble cloud. Acoustic B-mode imaging confirmed vaporization in the focal region within 10–20 ms of HIFU exposure at 2, 3, and 4 MPa [Fig. 3(A)]. No significant vaporization was observed prior to 10 ms of HIFU exposure at any pressure. No vaporization could be detected when HIFU was applied at a pressure of 1 MPa (corresponding to an intensity of 30 W/cm^2) regardless of the nanodroplet concentration. The mean pixel intensity within the acoustic focal area was measured as a function of pulse length [Fig. 3(B)]. Nanodroplets within the path of the beam but outside the focal spot did not experience sufficient pressure or heating to vaporize. HIFU delivered at 4 MPa resulted in a vaporization field (microbubble cloud) that was significantly larger than the corresponding ablation lesion that was formed within it (400 vs 150 mm^3).

C. Vaporization field volume

Vaporization field volumes were measured as a function of nanodroplet concentration and acoustic pressure [Fig. 3(C)]. The vaporization field volume increased both with increasing nanodroplet concentration and with the application of higher acoustic pressures. Applying continuous wave HIFU at 1 MHz for 20 s with a PNP of 4 MPa to a phantom containing 1 μl of the stock nanodroplet solution per milliliter produced a vaporization field volume of approximately 400 mm^3. At 2 MPa, the vaporization field volume was approximately 100 mm^3 [Fig. 3(C)]. No vaporization field could be detected in control phantoms (containing no nanodroplets) below 4 MPa.

D. Ablation lesion volume

Ablation lesion volumes were measured as a function of nanodroplet and microbubble concentration and acoustic pressure (Fig. 4). HIFU at 1 MPa for 20 s did not result in ablation lesion formation at any tested nanodroplet or microbubble concentration. At least 2 MPa of pressure was required to induce ablation. The volumes of the ablation lesions were highly dependent on the concentration of nanodroplets and microbubbles in the tissue-mimicking phantom and also on the PNP of insonation. For each acoustic pressure applied, ablation lesion volumes increased over several orders of magnitude of increasing nanodroplet (0–1 μl/ml) and microbubble (0–0.1 μl/ml) concentrations (Fig. 5). However, there were significant differences between the volumes of ablation lesions produced in phantoms containing nanodroplets compared to microbubbles. For each pressure,

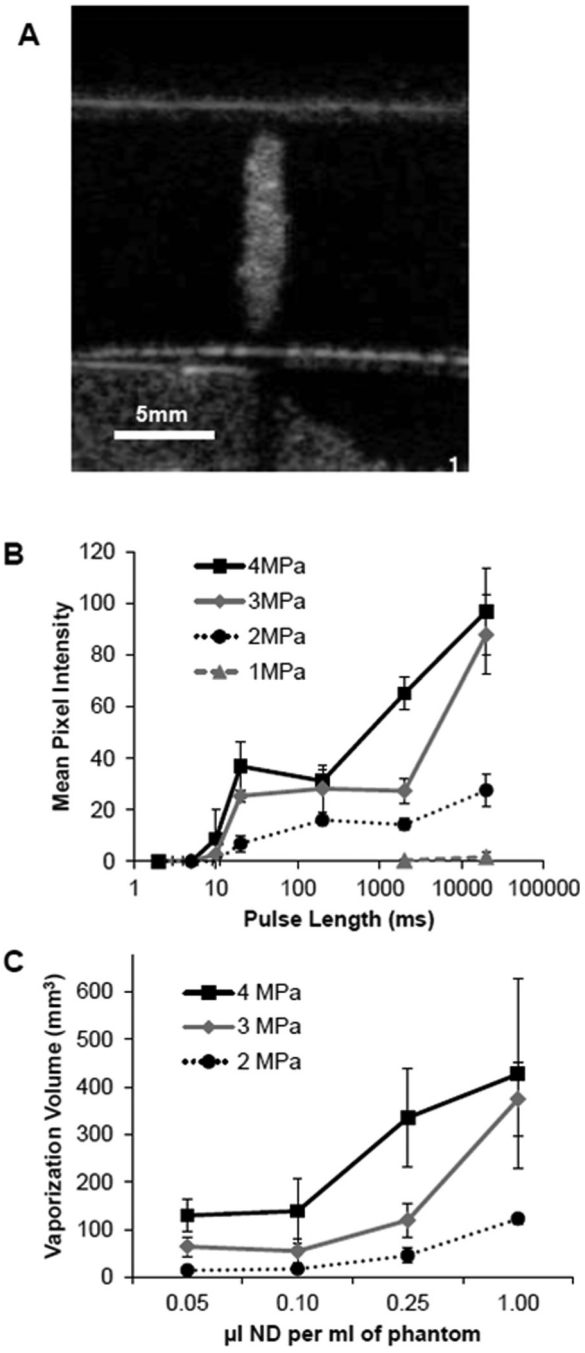

FIG. 3. Vaporization of nanodroplets in tissue-mimicking phantoms. (A) Representative acoustic image of vaporized nanodroplets in a phantom containing 0.1 μl of stock solution per milliliter. Notice no vaporization is present outside the focal zone or in the cap. An ellipse region of interest (ROI) measuring 1.5 mm × 10 mm was measured at the site of vaporization. (B) Mean pixel intensity within the ROI was assessed in phantoms containing 0.1 μl of nanodroplet stock per milliliter as a function of pulse length ($n \geq 3$, mean ± s.d.). (C) Vaporization volume resulting from 20 s of HIFU as a function of nanodroplet concentration over a range of pressure from 2-4 MPa ($n \geq 3$, mean ± s.d.).

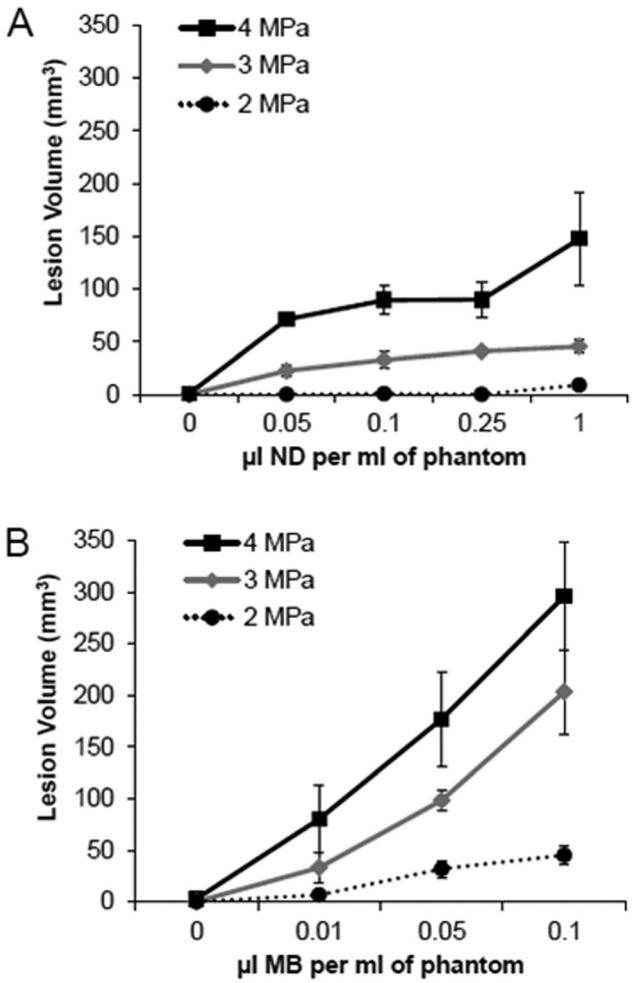

FIG. 4. Ablation lesion volume as a function of (A) nanodroplet (ND) or (B) microbubble (MB) concentration. Lesion volumes resulted from 20 s of HIFU at 2, 3, or 4 MPa ($n \geq 3$, mean ± s.d.).

the presence of microbubbles resulted in larger lesions than nanodroplets. At 4 MPa, ablation lesions achieved a peak average volume of approximately 300 mm^3 in phantoms containing microbubbles compared to a maximum volume approaching 150 mm^3 with nanodroplets. Maximum ablation lesion volume was achieved with microbubbles at a concentration that was a full order of magnitude lower than the required nanodroplet concentration (0.1 vs 1 μl/ml) to reach the same ablation volume. Even at low concentrations, both agents enhanced lesion volume. Microbubbles or nanodroplets at the 0.01 μl/ml concentration (0.1×10^6 per cm^3) resulted in mean lesion volumes of 80.4 ± 33.1 and 52.8 ± 14.2 mm^3 (mean ± s.e.), respectively, after 20 s of continuous 1 MHz HIFU at a PNP of 4 MPa (Fig. 5). In comparison, lesion volumes of 1.0 ± 0.8 mm^3 were generated in agent-free control phantoms under the same HIFU parameters. Lesion volume continually increased with increasing nanodroplet concentration over the entire range investigated. However, this was not true in phantoms containing microbubbles. The lesion volume decreased in phantoms containing more than 0.1 μl of microbubble stock per ml [Fig. 5(C)]. Eventually at concentrations of microbubbles greater than 1 μl/ml, ablation lesions formed only at the surface of the phantom and were too flat to accurately measure. As such, no data on these concentrations are presented.

E. Ablation lesion geometry and location

Differences in the shape of the ablation lesions produced by nanodroplet or microbubble-enhanced HIFU, as well as differences in the location of these lesions within the phantom, were analyzed by direct visualization and lesion measurement. The ideal lesion is a prolate ellipsoid (vertical axis > lateral axis) centered at the HIFU focal point. However, with increasing microbubble concentrations, the vertical axis of the ablation lesion shortens while the lateral

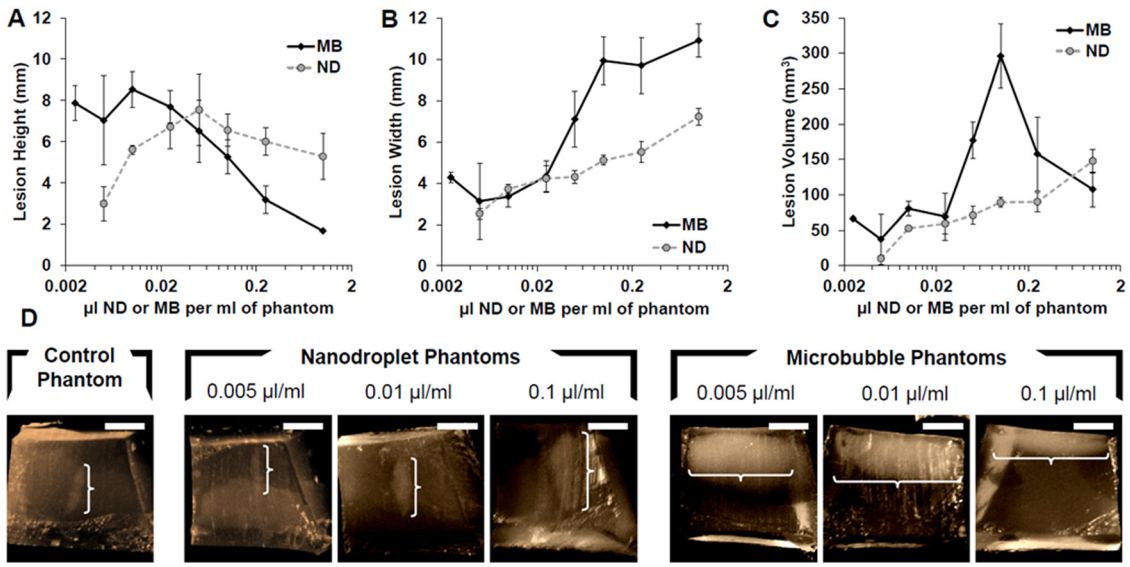

FIG. 5. (Color online) Ablation lesion height (A), width (B), and corresponding volume (C) as a function of ND or MB concentration in tissue-mimicking phantoms following HIFU exposure for 20 s at 4 MPa PNP. (D) Representative images of lesions formed inside the AAPs containing no agents, ND, or MB at various concentrations. The location and size of each lesion is indicated by the superimposed white bracket. The white scale bar in the upper right corner of each image represents 5 mm.

axis widens [Figs. 5(A) and 5(B)]. The resultant lesions are more oblate rather than prolate ellipsoids as microbubble concentrations increase. This oblate geometry occurs in phantoms with microbubble concentrations above 0.005 μl/ml and occurs at the frontal surface of the phantom not around the desired focal point at the center of the phantom [Fig. 5(D)]. At a microbubble concentration of 0.1 μl/ml, the largest ablation lesions were produced [Fig. 5(C)], but they were spread out over the phantom surface [Fig. 5(D)]. In contrast, lesions produced in nanodroplet phantoms retained their desired prolate shape for a greater range of concentrations [Fig. 5(D)]. These nanodroplet-associated prolate ellipsoids remained localized around the central focal point [Fig. 5(D)].

F. MR thermometry

MR thermometry was performed during the insonation of phantoms containing no (control) agents, 0.005 μl, or 0.01 μl of nanodroplets or microbubbles per milliliter by continuous wave HIFU for 60 s at 1 MHz and a PNP of 4.69 MPa. MR data were collected every 2.5 s during and for another 60 s following ablation. At each time point, the maximum intensity pixel along with its eight surrounding pixels was averaged to obtain the localized maximum change in temperature and is referred to as the "maximal temperature change" from here on. The maximal temperature change anywhere in the phantom over the 2 min data collection period was determined from vertical MR slices [Fig. 6(A)]. The maximal changes in temperature at the acoustic focus (ROI) and at the surface of the phantom were detected from the horizontal MR slices acquired at each corresponding plane [Figs. 6(B) and 6(C)].

Of all five types of non-control phantoms investigated, HIFU ablation of the two containing 0.005 or 0.01 μl microbubbles per milliliter and the phantom containing 0.1 μl of nanodroplets per milliliter resulted in a significantly enhanced temperature rise over the control (white bar in graphs). However, it is important to note that the maximal temperature rise did not occur at the same location within each type of phantom (Fig. 7). The maximal temperature rise occurred near the surface in microbubble phantoms, whereas the phantoms that contained nanodroplets incurred a maximal temperature rise near the acoustic focus in the center of the phantom. Maximal change in temperature at the acoustic target site was enhanced by 16.9% and 37.0% by microbubbles and nanodroplets, respectively.

The temperature vs time curves (Fig. 8) acquired at the surface of the phantoms and at the acoustic focus in the middle of the phantoms clearly illustrate the differences in thermal energy deposition between the nanodroplet and microbubble phantoms of the same 0.01 μl/ml concentration. The temperature at the acoustic focus was highest in the nanodroplet phantom and lowest in the control phantom. The peak temperature in the control phantoms was observed at the end of the HIFU application (60 s). The phantoms containing 0.01 μl of nanodroplets per milliliter reached the same temperature (15.4 °C) after only 20 s, thereby decreasing the ablation time needed. Minimal surface heating occurred in the nanodroplet phantoms and was only higher than the control after 40 s of ablation. The surface of the microbubble phantoms rose by more than 50° but only rose by about 19° at the targeted region of interest demonstrating that the majority of the heating occurred away from the intended target site.

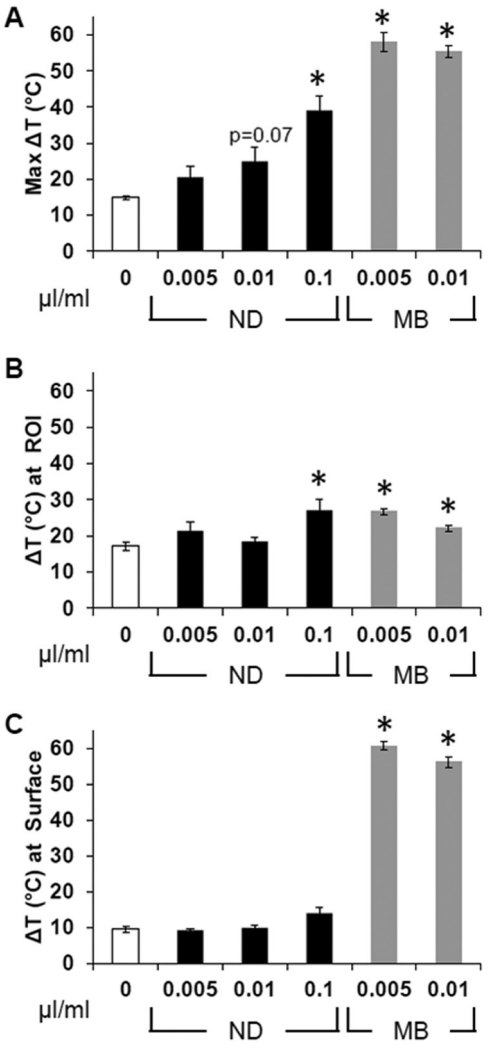

FIG. 6. Temperature change in AAPs after 60 s of continuous HIFU ablation at 20 W (4.69 MPa). The (A) maximal temperature change anywhere in the vertical cross section of the phantom, the (B) change in temperature at the location of the acoustic focus, and the (C) change in temperature at the surface of the phantom are all listed for each type of phantom and concentration of agents in microliters (mean ± s.e., *indicates $p \leq 0.05$ compared to 0 agents, $n \geq 3$).

IV. DISCUSSION

This study explored a novel phase-shift nanoagent for enhanced HIFU ablation. These phase-shift nanodroplets have a PFC core that combines highly volatile DFB with less-volatile DDFP. The goal of combining PFCs was to balance stability and acoustic sensitivity. By combining DFB and DDFP in a 1:1 mixture, vaporization and ablation was achieved at relatively low HIFU intensities, yet droplets were stable enough to remain intact in liquid form during phantom preparation and storage. The results of these studies demonstrated several advantages of these novel nanodroplets

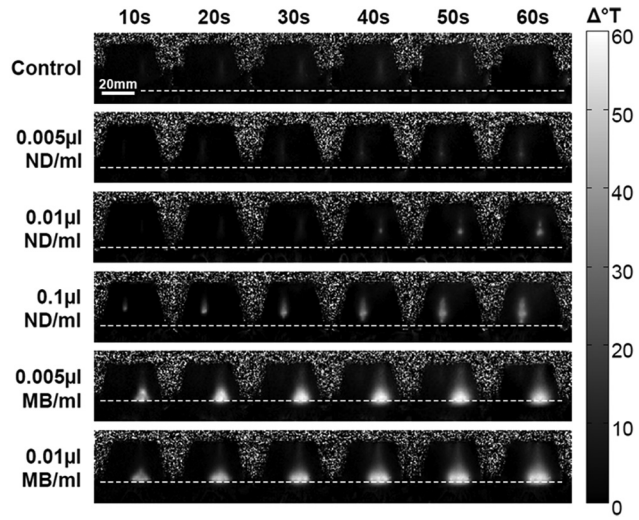

FIG. 7. MR thermometry maps of phantoms containing no agents (top row), ND (second to fourth rows) or MB (fifth and sixth rows). Frames shown were collected during the 60 s of HIFU ablation and indicate the intensity and location of the temperature change. The dotted line across each series of frames delineates the surface of the phantoms.

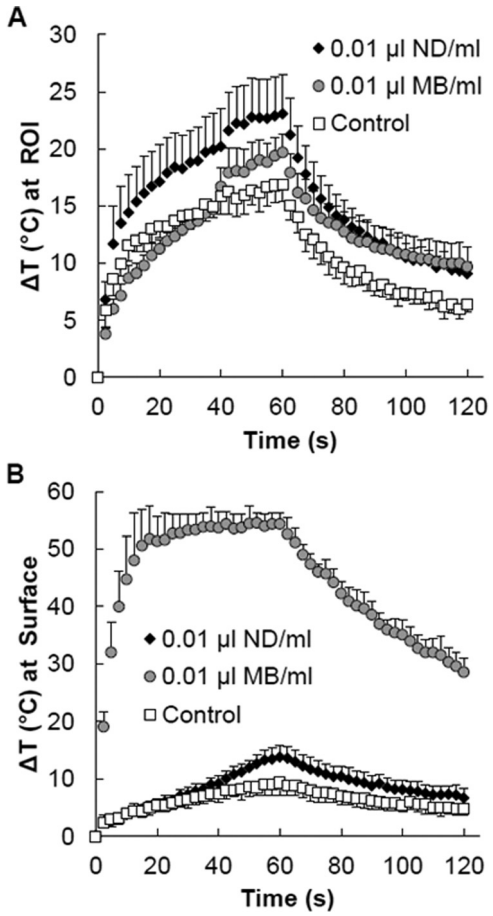

FIG. 8. For each MR acquisition over time, the maximum change in temperature (A) at the focus (ROI) and at the (B) surface of the phantom was extracted from the corresponding horizontal slices from those locations. Time curves were averaged, and data are presented as the means ± s.d. ($n \geq 3$). Phantoms contained 0.01 μl of ND/MB per milliliter of phantom material or no agents (control).

compared to gaseous PFC microbubbles—the clinical gold standard for acoustic contrast imaging.

Vaporization of the PFC nanodroplets into microbubbles was detected by acoustic imaging of the microbubble cloud. The vaporization field volume results from the interdependent effects of the acoustic beam geometry and pressure (intensity), temperature rise in the acoustic field, and the concentration of nanodroplets. The vaporization volume increased with increasing pulse length as was also reported previously by others (Lo *et al.*, 2007). However, at a sonication pressure of 4 MPa, large variability in the vaporization field volumes occurred within the two highest nanodroplet concentrations. This variability demonstrates the loss of control over lesion size, shape, and location that occurs in the higher range of nanodroplet concentrations and acoustic pressures. To induce an acoustically detectable vaporization cloud from the nanodroplets, a pressure of at least 2 MPa (PNP) for more than 10 ms was required. This threshold is hypothesized to be one of the main reasons why unintended heating within the prefocal zone was minimized in phantoms containing nanodroplets. Indeed, prefocal surface heating in nanodroplet phantoms was not significantly greater than surface heating in control phantoms based on the MR thermometry results.

HIFU ablation lesions in phantoms containing either type of agent were statistically larger than control lesions, but microbubbles were associated with surface heating and loss of control over lesion placement with higher concentrations. Previous studies have reported changes in lesion geometry with increasing microbubble concentrations such that ablation lesions become oblate ellipsoids (lateral axis > vertical axis) massed at the frontal phantom surface (Tung *et al.*, 2006). In our study, continuous-wave HIFU (20 s at 1 MHz and 4 MPa) produced ablation lesions with volumes averaging approximately 300 mm^3 in phantoms containing microbubbles. Lesions of similar volume have been reported in animal models of microbubble-enhanced HIFU ablation. Kaneko *et al.* (2005) demonstrated ablation lesions averaging almost 400 mm^3 in rabbit liver in response to 60 s of HIFU at an intensity of 400 W/cm^2 using air-based Levovist®. However, these large lesions may not be desirable. Tung *et al.* (2006) explored microbubble-enhanced HIFU ablation using Definity, a gaseous perfluoropropane contrast agent, in acrylamide-albumin gels. Although ablation lesions were significantly larger in microbubble-containing phantoms compared to control, undesirable changes in ablation lesion shape and location occurred with increasing microbubble concentrations. At lower microbubble concentrations, prolate ellipsoid ablation lesions were centered at the HIFU focal point. As microbubble concentrations increased, larger ablation lesions became asymmetric ellipsoids that migrated as much as 2 cm away from the focal point toward the ultrasound source. Finally, at the highest microbubble concentrations, the ablation lesions flattened along the frontal phantom surface and "shadowed" deeper sites such that no ablation occurred at the desired focal point. The largest microbubble mediated ablation lesions were achieved at a price of lost control over lesion geometry and location both in Tung's study and in this study.

Liquid nanodroplets offered advantages over microbubbles when exposed to HIFU in the tissue-mimicking model. For a given concentration or pressure, lesions in response to nanodroplets were significantly smaller than microbubble-associated lesions. However, ablation lesions produced in the presence of nanodroplets were less prone to shape change and lesion migration than microbubble-enhanced lesions. MR thermometry maps of phantoms containing nanodroplets revealed HIFU heating in the phantom center and not at its surface. The MR thermometry studies were performed at room temperature because it was not straightforward to heat the phantoms to 37° inside the MR scanner. So it is possible that the nanodroplets were not performing optimally. Vaporization is dependent both on acoustic parameters and the ambient temperature. Even greater thermal enhancement is therefore expected to occur during HIFU ablation of nanodroplets at body temperature. Regardless, the results suggest that the energy required to achieve phase transition of our novel liquid nanodroplet provides the opportunity to control the size and placement of ablation lesions during PFC-enhanced HIFU.

Although we are working with nanodroplets, it is notable that the number of agents required to enhance ablation in our studies is comparable to the number of microbubbles injected during contrast imaging with Definity; this makes the use of this technology more clinically feasible. In this study, the presence of PFC nanodroplets in the tissue-mimicking phantoms resulted in larger HIFU-induced ablation lesions than could be achieved in control phantoms without agent. Previous studies have also reported enhanced HIFU ablation using liquid PFC droplets. Zhang *et al.* (2011) demonstrated ablation lesions with volumes approaching 600 mm^3 in tissue-mimicking acrylamide phantoms containing an estimated concentration of 3×10^5 DDFP droplets/ml after 5 s of HIFU. Although these lesions are notably larger than the ablation lesions reported in our study, despite the shorter insonation time and the use of pure, less-volatile DDFP, it should be noted that the droplets were micron-sized and HIFU was applied at an intensity of 4000 W/cm^2. The differences in the results highlight the fact that the final ablation response during PFC-enhanced HIFU depends on many factors, including PFC droplet characteristics (boiling point, size, and concentration) as well as acoustic parameters (intensity and exposure duration).

Our studies demonstrate that by controlling vaporization, the location of enhanced thermal energy deposition can be controlled. Whereas microbubbles impede the acoustic beam causing surface lesions and "shadowing" of the beam, the nanodroplets do not impede the beam prior to vaporization and allow for deeper lesion generation. We expect our nanodroplets to be capable of extravasating due to their 100–300 nm diameters; however, this will be the focus of future studies. Benefits of nanodroplet-enhanced HIFU include shorter treatment times, decreased risk to healthy tissue along the ultrasound path, and deeper access to tumors.

V. CONCLUSIONS

Our nanodroplet formulation offers several advantages over microbubbles for HIFU ablation procedures. Microbubble-enhanced HIFU ablation is complicated by surface and non-targeted heating. In contrast, our nanodroplet formulation does not substantially enhance thermal energy deposition prior to vaporization. Because the nanodroplets require sufficient energy for vaporization, targeted ablation can be achieved at the focal point of the transducer inside deep tissue. Nanodroplets were found to reduce the acoustic energy and time required to ablate a tissue mimicking material. As such, these nanodroplets have the potential both to reduce the procedure time and to improve the safety of focused ultrasound surgery.

ACKNOWLEDGMENTS

The authors would like to thank Dr. Richard Price and Kelsie Timbie for their help and expertise with the MR-compatible focused ultrasound system used in the thermometry studies and also Dr. Natalia Lebedeva for assistance with acrylamide phantoms. Funding support was provided by NIGMS: SPIRE Postdoctoral Fellowship to L.C.P., a NSF graduate fellowship to P.S.S., and a UNC-SURF fellowship to C.P. We also acknowledge the support of NIH Grant No. EB-011704 (T.O.M.), funding from the Carolina Center for Cancer Nanotechnology Excellence (P.A.D.), and pilot funds from NSF DMR#1122483 (P.A.D.).

Chomas, J. E., Dayton, P., Allen, J., Morgan, K., and Ferrara, K. W. (**2001a**). "Mechanisms of contrast agent destruction," IEEE Trans. Ultrason. Ferroelectr. Freq. Control **48**, 232–248.

Chomas, J. E., Dayton, P., May, D., and Ferrara, K. (**2001b**). "Threshold of fragmentation for ultrasonic contrast agents," J. Biomed. Opt. **6**, 141–150.

Connor, C. W., and Hynynen, K. (**2004**). "Patterns of thermal deposition in the skull during transcranial focused ultrasound surgery," IEEE Trans. Biomed. Eng. **51**, 1693–1706.

Coussios, C. C., Farny, C. H., Ter Haar, G., and Roy, R. A. (**2007**). "Role of acoustic cavitation in the delivery and monitoring of cancer treatment by high-intensity focused ultrasound (HIFU)," Int. J. Hypertherm. **23**, 105–120.

Dayton, P. A., Morgan, K. E., Klibanov, A. L., Brandenburger, G. H., and Ferrara, K. W. (**1999**). "Optical and acoustical observations of the effects of ultrasound on contrast agents," IEEE Trans. Ultrason. Ferroelectr. Freq. Control **46**, 220–232.

Ferrara, K., Pollard, R., and Bordeni, M. (**2007**). "Ultrasound microbubble contrast agents: Fundamentals and application to gene and drug delivery," Annu. Rev. Biomed. Eng. **9**, 415–447.

Fischer, K., Gedroyc, W., and Jolesz, F. A. (**2010**). "Focused ultrasound as a local therapy for liver cancer," Cancer J. **16**, 118–124.

Ganan-Calvo, A. M. (**2004**). "Perfectly monodisperse microbubbling by capillary flow focusing: An alternate physical description and universal scaling," Phys. Rev. E **69**, 027301.

Gedroyc, W. M. W., and Anstee, A. (**2007**). "MR-guided focused ultrasound," Expert Rev. Med. Devices **4**, 539–547.

Germain, D., Chevallier, P., Laurent, A., and Saint-Jalmes, H. (**2001**). "MR monitoring of tumour thermal therapy," Magn. Reson. Mater. Phys., Biol., Med. **13**, 47–59.

Goldberg, B. B., Liu, J. B., and Forsberg, F. (**1994**). "Ultrasound contrast agents: A review," Ultrasound Med. Biol. **20**, 319–333.

Hill, C. R., and terHaar, G. R. (**1995**). "Review article: High intensity focused ultrasound-potential for cancer treatment," Br. J. Radiol. **68**, 1296–1303.

Hindman, J. C. (**1966**). "Proton resonance shift of water in gas and liquid states," J. Chem. Phys. **44**, 4582–4592.

Ishihara, Y., Calderon, A., Watanabe, H., Okamoto, K., Suzuki, Y., and Kuroda, K. (**1995**). "Precise and fast temperature mapping using water proton chemical-shift," Magn. Reson. Med. **34**, 814–823.

Jang, H. J., Lee, J.-Y., Lee, D.-H., Kim, W.-H., and Hwang, J. H. (**2010**). "Current and future clinical applications of high-intensity focused ultrasound (HIFU) for pancreatic cancer," Gut Liver **4**, S57–S61.

Kaneko, Y., Maruyama, T., Takegami, K., Watanabe, T., Mitsui, H., Hanajiri, K., Nagawa, H. A., and Matsumoto, Y. (**2005**). "Use of a microbubble agent to increase the effects of high intensity focused ultrasound on liver tissue," Eur. Radiol. **15**, 1415–1420.

Kawabata, K.-I., Asami, R., Azuma, T., and Umemura, S.-I. (**2010**). "Acoustic response of microbubbles derived from phase-change nanodroplet," Jpn. J. Appl. Phys. **49**, 07HF16.

Kennedy, J. E. (**2005**). "High-intensity focused ultrasound in the treatment of solid tumours," Nat. Rev. Cancer **5**, 321–327.

Kinsey, A. M., Diederich, C. J., Rieke, V., Nau, W. H., Pauly, K. B., Bouley, D., and Sommer, G. (**2008**). "Transurethral ultrasound applicators with dynamic multi-sector control for prostate thermal therapy: In vivo evaluation under MR guidance," Med. Phys. **35**, 2081–2093.

Kripfgans, O. D., Fowlkes, J. B., Woydt, M., Eldevik, O. P., and Carson, P. L. (**2002**). "In vivo droplet vaporization for occlusion therapy and phase aberration correction," IEEE Trans. Ultrason. Ferroelectr. Freq. Control **49**, 726–738.

Kripfgans, O. D., Orifici, C. M., Carson, P. L., Ives, K. A., Eldevik, O. P., and Fowlkes, J. B. (**2005**). "Acoustic droplet vaporization for temporal and spatial control of tissue occlusion: A kidney study," IEEE Trans. Ultrason. Ferroelectr. Freq. Control **52**, 1101–1110.

Kyriakou, Z., Ignasi Corral-Baques, M., Amat, A., and Coussios, C.-C. (**2011**). "HIFU-induced cavitation and heating ex vivo porcine subcutaneous fat," Ultrasound Med. Biol. **37**, 568–579.

Liberman, B., Gianfelice, D., Inbar, Y., Beck, A., Rabin, T., Shabshin, N., Chander, G., Hengst, S., Pfeffer, R., Chechick, A., Hanannel, A., Dogadkin, O., and Catane, R. (**2009**). "Pain palliation in patients with bone metastases using mr-guided focused ultrasound surgery: A multicenter study," Ann. Surg. Oncol. **16**, 140–146.

Liu, H. L., Chen, W. S., Chen, J. S., Shih, T. C., Chen, Y. Y., and Lin, W. L. (**2006**). "Cavitation-enhanced ultrasound thermal therapy by combined low- and high-frequency ultrasound exposure," Ultrasound Med. Biol. **32**, 759–767.

Lo, A. H., Kripfgans, O. D., Carson, P. L., Rothman, E. D., and Fowlkes, J. B. (**2007**). "Acoustic droplet vaporization threshold: Effects of pulse duration and contrast agent," IEEE Trans. Ultrason. Ferroelectr. Freq. Control **54**, 933–946.

Lukka, H., Waldron, T., Chin, J., Mayhew, L., Warde, P., Winquist, E., Rodrigues, G., Shayegan, B., and Canc Care Ontarios, P. (**2011**). "High-intensity focused ultrasound for prostate cancer: A systematic review," Clin. Oncol. **23**, 117–127.

Maleke, C., and Konofagou, E. E. (**2008**). "Harmonic motion imaging for focused ultrasound (HMIFU): A fully integrated technique for sonication and monitoring of thermal ablation in tissues," Phys. Med. Biol. **53**, 1773–1793.

Maleke, C., and Konofagou, E. E. (**2010**). "In vivo feasibility of real-time monitoring of focused ultrasound surgery (FUS) using harmonic motion imaging (HMI)," IEEE Trans. Biomed. Eng. **57**, 7–11.

McDannold, N., Clement, G. T., Black, P., Jolesz, F., and Hynynen, K. (**2010**). "Transcranial magnetic resonance imaging-guided focused ultrasound surgery of brain tumors: Initial findings in 3 patients," Neurosurgery **66**, 323–332.

McDannold, N., King, R. L., and Hynynen, K. (**2004**). "MRI monitoring of heating produced by ultrasound absorption in the skull: In vivo study in pigs," Magn. Reson. Med. **51**, 1061–1065.

Mougenot, C., Kohler, M. O., Enholm, J., Quesson, B., and Moonen, C. (**2011**). "Quantification of near-field heating during volumetric MR-HIFU ablation," Med. Phys. **38**, 272–282.

Mullin, L., Gessner, R., Kwan, J., Kaya, M., Borden, M. A., and Dayton, P. A. (**2011**). "Effect of anesthesia carrier gas on in vivo circulation times of ultrasound microbubble contrast agents in rats," Contrast Med. Mol. Imaging **6**, 126–131.

Pauly, K. B., Diederich, C. J., Rieke, V., Bouley, D., Chen, J., Nau, W. H., Ross, A. B., Kinsey, A. M., and Sommer, G. (**2006**). "Magnetic resonance-guided high-intensity ultrasound ablation of the prostate," Top. Magn. Reson. Imaging **17**, 195–207.

Rapoport, N., Nam, K.-H., Christensen, D. A., and Kennedy, A. M. (**2010**). "Ultrasound-mediated tumor chemotherapy with drug-loaded phase-shift nanoemulsions," J. Acoust. Soc. Am. **127**, 1976–1976.

Rapoport, N., Nam, K. H., Gupta, R., Gao, Z. G., Mohan, P., Payne, A., Todd, N., Liu, X., Kim, T., Shea, J., Scaife, C., Parker, D. L., Jeong, E. K., and Kennedy, A. M. (**2011**). "Ultrasound-mediated tumor imaging and nanotherapy using drug loaded, block copolymer stabilized perfluorocarbon nanoemulsions," J. Controlled Release **153**, 4–15.

Rapoport, N. Y., Kennedy, A. M., Shea, J. E., Scaife, C. L., and Nam, K. H. (**2009**). "Controlled and targeted tumor chemotherapy by ultrasound-activated nanoemulsions/microbubbles," J. Controlled Release **138**, 268–276.

Reznik, N., Williams, R., and Burns, P. N. (**2011**). "Investigation of vaporized submicron perfluorocarbon droplets as an ultrasound contrast agent," Ultrasound Med. Biol. **37**, 1271–1279.

Rieke, V., and Pauly, K. B. (**2008**). "MR thermometry," J. Magn. Reson. Imaging **27**, 376–390.

Ringold, S. (**2004**). "FDA approves ultrasound fibroid therapy," J. Am. Med. Assoc. **292**, 2826.

Sheeran, P. S., and Dayton, P. A. (**2012**). "Phase-change contrast agents for imaging and therapy," Curr. Pharm. Des. **18**, 2152–2165.

Sheeran, P. S., Luois, S., Dayton, P. A., and Matsunaga, T. O. (**2011a**). "Formulation and Acoustic studies of a new phase-shift agent for diagnostic and therapeutic ultrasound," Langmuir **27**, 10412–10420.

Sheeran, P. S., Luois, S. H., Mullin, L. B., Matsunaga, T. O., and Dayton, P. A. (**2012**). "Design of ultrasonically activatable nanoparticles using low boiling point perfluorocarbons," Biomaterials **33**, 3262–3269.

Sheeran, P. S., Wong, V. P., Luois, S., McFarland, R. J., Ross, W. D., Feingold, S., Matsunaga, T. O., and Dayton, P. A. (**2011b**). "Decafluorobutane as a phase-change contrast agent for low-energy extravascular ultrasonic imaging," Ultrasound Med. Biol. **37**, 1518–1530.

Singh, R., Husseini, G. A., and Pitt, W. G. (**2012**). "Phase transitions of nanoemulsions using ultrasound: Experimental observations," Ultrason. Sonochem. **19**, 1120–1125.

Stride, E. P., and Coussios, C. C. (**2010**). "Cavitation and contrast: The use of bubbles in ultrasound imaging and therapy," Proc. Inst. Mech. Eng., Part H: J. Eng. Med. **224**, 171–191.

Takegami, K., Kaneko, Y., Watanabe, T., Maruyama, T., Matsumoto, Y., and Nagawa, H. (**2004**). "Polyacrylamide gel containing egg white as new model for irradiation experiments using focused ultrasound," Ultrasound Med Biol **30**, 1419–1422.

Talu, E., Lozano, M. M., Powell, R. L., Dayton, P. A., and Longo, M. L. (**2006**). "Long-term stability by lipid coating monodisperse microbubbles formed by a flow-focusing device," Langmuir **22**, 9487–9490.

Tempany, C. M. C., McDannold, N. J., Hynynen, K., and Jolesz, F. A. (**2011**). "Focused ultrasound surgery in oncology: Overview and principles," Radiology **259**, 39–56.

Tran, B. C., Seo, J., Hall, T. L., Fowlkes, J. B., and Cain, C. A. (**2003**). "Microbubble-enhanced cavitation for noninvasive ultrasound surgery," IEEE Trans. Ultrason. Ferroelectr. Frequency Control **50**, 1296–1304.

Tung, Y.-S., Liu, H.-L., Wu, C.-C., Ju, K.-C., Chen, W.-S., and Lin, W.-L. (**2006**). "Contrast-agent-enhanced ultrasound thermal ablation," Ultrasound Med Biol. **32**, 1103–1110.

Villanueva, F. S. (**2008**). "Molecular imaging of cardiovascular disease using ultrasound," J. Nucl. Cardiol. **15**, 576–586.

Wu, F., ter Haar, G., and Chen, W. R. (**2007**). "High-intensity focused ultrasound ablation of breast cancer," Expert Rev. Anticancer Therapy **7**, 823–831.

Xu, J. H., Li, S., Chen, G. G., and Luo, G. S. (**2006**). "Formation of monodisperse microbubbles in a microfluidic device," Aiche J. **52**, 2254–2259.

Xu, Z., Fowlkes, J. B., Rothman, E. D., Levin, A. M., and Cain, C. A. (**2005**). "Controlled ultrasound tissue erosion: The role of dynamic interaction between insonation and microbubble activity," J. Acoust. Soc.A. **117**, 424–435.

Yu, T. H., Fan, X. L., Xiong, S. H., Hu, K., and Wang, Z. B. (**2006a**). "Microbubbles assist goat liver ablation by high intensity focused ultrasound," Eur. Rad. **16**, 1557–1563.

Yu, T. H., Xiong, S. H., Mason, T. J., and Wang, Z. B. (**2006b**). "The use of a microbubble agent to enhance rabbit liver destruction using high intensity focused ultrasound," Ultrason. Sonochem. **13**, 143–149.

Zhang, M., Fabiilli, M. L., Haworth, K. J., Padilla, F., Swanson, S. D., Kripfgans, O. D., Carson, P. L., and Fowlkes, J. B. (**2011**). "Acoustic droplet vaporization for enhancement of thermal ablation by high intensity focused ultrasound," Acad. Radiol. **18**, 1123–1132.

Zhang, P., and Porter, T. (**2010**). "An in vitro study of a phase-shift nanoemulsion: A potential nucleation agent for bubble-enhanced HIFU tumor ablation," Ultrasound Med. Biol. **36**, 1856–1866.